Direct-Conversion Spectrum Sensor Impaired by Symmetric α-Stable and α-Sub-Gaussian Noises

Luiz Gustavo Barros Guedes and Dayan Adionel Guimarães

***Abstract*—Spectrum sensing in underwater cognitive acoustic networks or in underwater acoustic sensor networks can be impaired by impulsive noise generated by snapping shrimps. In mathematical analysis or simulations, the amplitude variations of this noise are commonly modeled by the symmetric alpha-stable (SαS) distribution. As an alternative, the alpha-sub-Gaussian (αSG) distribution can model both temporal correlation and amplitude variations. This article assesses the performance of underwater spectrum sensing with a direct-conversion receiver (DCR) under impulsive noise modeled by the SαS and αSG distributions. Several recent test statistics are compared, demonstrating that they have different degrees of robustness against impulsive noise and that the DCR is significantly less sensitive to this noise, compared to the conventional receiver model that does not take into account the influences of hardware characteristics into the performance of spectrum sensing.**

***Index Terms*—Spectrum sensing, direct-conversion receiver, impulsive noise, underwater communications, snapping shrimp, SαS, αSG.**

I. Introduction

NOWADAYS, the fixed bandwidth allocation policy governs the use of the radiofrequency (RF) spectrum, allocating a certain RF band only to the user who contracts it, also known as the primary user (PU). Owed to this policy, spectrum scarcity and underutilization are experienced. The scarcity refers to the lack of new free bands. Moreover, once the PU is not using it, that band becomes momentarily unoccupied and the frequency spectrum becomes underutilized.

Massive connection among different devices is foreseen for future communication networks [1], requiring a better use of spectrum bands for the proper accommodation of the expected large number of transmitters and receivers. There is also an increase in demand for new telecommunications services, which in the context of a fixed bandwidth allocation policy, exacerbates the problem of spectrum scarcity and underutilization.

A possible alternative to this problem is the adoption of a dynamic spectrum allocation policy, implemented through secondary networks of cognitive radios performing spectrum sensing [2], [3]. In this way, an opportunistic use of the spectrum is sought, so that an unlicensed user, also known as a secondary user (SU), seeks for occasions of shared transmission with the PU, in an overlapping manner or not, on licensed bands that are, for example, temporarily out of use.

In underwater communication systems [4], the problem of spectrum scarcity is also present, which is intensified by the fact that services are allocated in a more restricted operating frequency range, between tens of Hertz and hundreds of kilohertz. In this context, the present work has as motivation the dynamic spectrum access (DSA) in underwater cognitive acoustic networks (UCANs) [5]–[7] or in underwater acoustic sensor networks (UASNs) [8]. DSA addresses the efficient occupation of spectrum bands both in the spatial (different locations) and temporal (different moments) domains, with the former associated to the positions of the spectrum sensors and the latter associated to the spectrum sensing events over time.

Not only multipath propagation, but also the various forms of interference and noise can affect the performance of spectrum sensing. Concerning the noise, its ubiquitous form in communication systems is the additive white Gaussian noise (AWGN). Furthermore, in certain environments, sporadic signals having short duration and high amplitude characterize a phenomenon called impulsive noise [9], [10].

Although the aforementioned impairments affect the performance of underwater communications and underwater spectrum sensing, the impulsive noise caused by snapping shrimps [4] deserves especial attention in the context of UCANs based on acoustic signals, since it is capable of producing severe performance degradation. On the other hand, the correct assessment of its impact must be addressed, since different receiver models can exhibit different degrees of robustness against the snapping shrimp noise.

The snapping shrimp noise is generated by a crustacean which, when quickly closing the larger of its two pincer-shaped claws, produces, in its front part, a high-velocity jet of water responsible for inducing a sudden pressure reduction in that region, resulting in the formation and consequent rupture of cavitation bubbles. This phenomenon generates high-intensity acoustic noise, sufficient to cause severe disturbances in underwater acoustic communications.

The level of performance degradation imposed by the snapping shrimp noise is related to the way the spectrum sensor is constructed. In the spectrum sensing literature, a conventional receiver model is the one that does not consider any signal processing stage determined by actual reception circuits. Thus, it is of great practical appeal to assess the performance in receivers with more realistic architectures for processing the received signal. In this work, a direct-conversion receiver

Luiz G. B. Guedes and Dayan A. Guimarães, National Institute of Telecommunications (*Instituto Nacional de Telecomunicações*, Inatel), Santa Rita do Sapucaí - MG, e-mail: luiz.guedes@mtel.inatel.br, dayan@inatel.br, ORCID: 0000-0002-1823-4812, 0000-0002-1304-792X.

This work was supported in part by RNP, with resources from MCTIC, Grant No. No 01245.010604/2020-14, under the Brazil 6G project of the Radiocommunication Reference Center (*Centro de Referência em Radiocomunicações*, CRR) of the National Institute of Telecommunications (*Instituto Nacional de Telecomunicações*, Inatel), and in part by CNPq, Brazil.
doi: 10.14209/jcis.2023.5.

(DCR) architecture is adopted due to its attractiveness for circuit integration in practice [11]–[13].

Commonly, in mathematical analysis and simulations, the snapping shrimp noise is modeled through temporally uncorrelated samples, following the symmetric alpha-stable (SαS) distribution [9], [14]. However, it is suspected that the SαS distribution is not the most suitable choice, which has been also verified, for instance, in [15]–[17]. This is owed to the fact that the snapping shrimp noise samples exhibit a temporal correlation that is not present in SαS samples. As an alternative, the alpha-sub-Gaussian (αSG) distribution [15], [16] can be used, modeling the amplitude variations as well as the temporal correlation existing in the impulsive phenomena.

Hence, it is of scientific interest to address the performance of detectors for spectrum sensing when impaired by impulsive noise. Moreover, it is of paramount importance to match the impulsive noise model to the corresponding noise source, aiming at obtaining trustable results and analyses. Finally, it is relevant to model the receiver adopted for spectrum sensing according to the signal processing tasks carried out in actual receivers. The present work tackles all these aspects.

A. Related research

Referring to the distributions for impulsive noise modeling, [18] proposes a theoretical analysis of the performance of the energy detector in channels with fading and impulsive noise, the latter characterized by a Bernoulli-Gaussian model. According to the authors, this model has significant practical appeal in multicarrier transmission systems based on orthogonal frequency division multiplexing.

The work developed in [19] proposes a spectrum sensing scheme with a hyperbolic tangent-based energy detector (HT-ED) in order to improve the performance under non-Gaussian noise, such as impulsive noise. Two distributions are used in modeling this type of noise: Laplace and SαS.

It has been found that the SαS distribution is widely used in impulsive noise modeling in the most recent articles that analyze the performance of spectrum sensing in cognitive radio networks. References [20]–[25] are cited as examples. In [17], the adequacy of the SαS distribution is analyzed in contrast to the αSG distribution with non-zero temporal correlation, in the context of underwater spectrum sensing subjected to snapping shrimp noise.

As for the receiver model, in [12] a direct-conversion receiver model is proposed considering realistic aspects in its implementation. The motivation for that work was the lack of research that points out the possible influences imposed by the reception circuit in the performance of systems intended for spectrum sensing, specifically in the case of centralized cooperative spectrum sensing with data fusion.

The model proposed in [12] has been improved in [13], aiming to better adapt it to direct-conversion receiver structures, commonly present in real software-defined radios (SDRs). In addition, it has been sought to improve the characteristics of the sensing channel model, making it more flexible through a channel with a random Rice factor [26, p. 212], as well as time-varying levels of noise and received signal powers.

The performance of spectrum sensing when impaired by impulsive noise is also evaluated in [27]. Two receivers are compared: a conventional one, which does not consider practical implementation aspects, and a DCR model that takes these aspects into account.

In [28] the performance analysis of test statistics based on eigenvalues is carried out under two approaches. The first considers the effects caused by impulsive noise and the second evaluates the performance of the system using both the direct-conversion receiver proposed in [12] and the conventional one. In the most recent articles which assess the performance of spectrum sensing in cognitive radio networks under impulsive noise, there is no mention to the use of a receiver model that considers realistic aspects in its implementation [22], [24].

Regarding studies on spectrum sensing in UCANs, a receiver-initiated spectrum management system and a dynamic control medium access control (MAC) channel are proposed in [29] to mitigate congestion in the common control channel. In [30], a new multi-layer algorithm for cooperative spectrum sensing, based on compressive sensing, is designed to estimate the spectrum in order to reduce the sampling rate and the header of acoustic signals. The main objective of [8] is to improve the accuracy of spectrum sensing by improving the use of the underwater frequency spectrum through a model based on energy detection with two thresholds and hard decision fusion, preventing attacks from malicious users. In [31], a protocol for cooperative underwater spectrum sharing for a centralized UCAN is proposed, consisting of two parts. The first one checks the random occurrence of interference periodically, by dividing the time domain into frames consisting of sensing and non-sensing subframes. The second part designs two heuristic resource allocation algorithms.

B. Contributions and organization of the article

In this article, the performance of spectrum sensing with the conventional receiver model is compared with the performance attained by the DCR-based model. These receivers are supposed to belong to a UCAN, thus being impaired by snapping shrimp impulsive noise. The influence of the impulsive noise statistics is also addressed by means of comparing its effect under the SαS and the αSG distributions. More specifically, the following investigations have been carried out:

- Study of the suitability of the SαS and αSG distributions for modeling the snapping shrimp noise through statistical analysis. Comparisons are made through the covariance matrices and the autocorrelation functions of the noise from SαS and αSG random number generators, as well as from an audio file of real snapping shrimp noise, obtained by data acquisition via hydrophone;
- Performance analysis of centralized cooperative spectrum sensing (CSS) with data fusion subjected to SαS and αSG noises. Conventional and DCR-based receiver models are used to compare the performances of the energy detector (ED), the absolute value cumulating (AVC) detector, the Gerschgorin radii and centers ratio (GRCR) detector, the Gini index detector (GID), the Pietra-Ricci index detector

(PRIDe) and the locally most powerful invariant test (LMPIT) detector.

This work merges and extends the research reported in [17] and [27]. The merged part refers to the assessment of the conventional and the DCR-based receiver models under SαS and αSG noise. The extended part refers to the addition of a large number of new results in which the spectrum sensing performance is measured as a function of the main system parameters, instead of using receiver operating characteristic (ROC) curves, for all detectors considered in [27] and [17], and for an additional detector, the AVC, claimed to be suitable for the impulsive noise scenario.

The remainder of the article is organized as follows: Section II addresses the distributions SαS and αSG, while Section III presents a statistical analysis of computer-generated noise samples following the SαS and αSG distributions and of real recorded audio of the snapping shrimp noise. Section IV is devoted to the models for the signals and systems adopted in the spectrum sensing scenario. Simulation results regarding the spectrum sensing performance are presented in Section V. Section VI concludes the work.

II. SαS AND αSG NOISE MODELS

The SαS noise (SαSN) is formed by independent and identically distributed samples from a particularization of the α-stable distribution. This distribution has no general closed form for its probability density function (PDF), but can be described by the characteristic function [32]

$$\Phi(\omega) = \exp\{j\delta\omega - \gamma|\omega|^{\alpha}[1 + j\beta\text{sign}(\omega)\kappa(\omega,\alpha)]\}, \quad (1)$$

wherein $\kappa(\omega,\alpha) = \tan(\pi\alpha/2)$ for $\alpha \neq 1$, or $\kappa(\omega,\alpha) = (2/\pi)\log|\omega|$ for $\alpha = 1$, and $\text{sign}(\cdot)$ corresponds to the sign function. The characteristic exponent $\alpha \in (0, 2]$ determines the degree of impulsivity, which is inversely proportional to its value. If $\alpha = 2$, the PDF α-stable becomes Gaussian. The scale parameter or scale factor $\gamma \in (0, \infty)$ controls the noise level, which is associated with the dispersion of the PDF, with a similar effect to the variance of a Gaussian distribution. The location parameter $\delta \in \mathbb{R}$ behaves similarly to the mean for symmetric distributions and to the median for skewed distributions. Finally, the symmetry parameter around δ is $\beta \in [-1, 1]$ [14].

Herein $\beta = 0$, yielding a symmetric PDF around δ, which is denoted as SαS distribution. Additionally considering $\delta = 0$, (1) especializes to the characteristic function of the SαS distribution. Such considerations culminates in the SαSN model, which can be viewed as an additive white Gaussian noise (AWGN) added to sporadic short-duration and high-amplitude peaks [14].

When used to mimic the snapping shrimp noise, the SαSN is unable to model the temporal correlation existing in this type of noise, even if it has adherence to its amplitude variations. The αSG distribution is a possible solution in terms of also modeling the temporal correlation. The characteristic function [15] of the αSG distribution is given by

$$\Phi_{\mathbf{w}}(\boldsymbol{\omega}) = \exp\left[-\left(\tfrac{1}{2}\boldsymbol{\omega}^{\mathrm{T}}\mathbf{M}\boldsymbol{\omega}\right)^{\frac{\alpha}{2}}\right], \quad (2)$$

where $\mathbf{w}$ represents the time series following the αSG distribution, $\boldsymbol{\omega} = [\omega_1\ \omega_2\ \cdots\ \omega_n]^{\mathrm{T}}$ is the n-dimensional independent variable and $\mathbf{M}$ denotes the covariance matrix of $\mathbf{w}$. The operator T indicates transposition.

The α-sub-Gaussian noise with memory of order ξ, which is hereafter denoted by the achronim αSGN(ξ), comes from the $(\xi+1)$-dimensional αSG distribution, corresponding to a subclass of the SαS distribution with $\delta = \beta = 0$, which can be represented by the time series $\mathbf{w}_{t,\xi} = \mathbf{w}_{\xi} = [w_{t-\xi}\ w_{t-\xi+1}\ \cdots\ w_t]^{\mathrm{T}}$ [15], [16]. This series corresponds to a window composed of $\xi + 1$ samples starting from the discrete-time instant t. Such noise is stationary and follows the SαS distribution for the amplitude of each sample, with any adjacent $\xi + 1$ samples following the αSG distribution, which ensures that exists a temporal correlation among them, which is determined by $\mathbf{M}$.

The αSGN(ξ), as described herein, is parameterized by α and by a symmetric Toeplitz covariance matrix, $\mathbf{M}$, independent of time. The scale factor γ is implicit in $\mathbf{M}$.

III. STATISTICAL ANALYSIS OF SαSN AND αSGN

This section reports an analysis of the autocorrelation function and the covariance matrix of time series formed by audio samples of a real snapping shrimp noise and by computer-generated αSGN(ξ) and SαSN samples.

The normalized discrete autocovariance function [33, p. 31] of the time series $\mathbf{x} = [x_1\ x_2\ \cdots\ x_n]^{\mathrm{T}}$ of real random variables is computed by Matlab via

$$C(k) = \frac{1}{\sigma_{\mathbf{x}}^2 n}\sum_{t=1}^{n-k}(x_t - \mu_{\mathbf{x}})(x_{t+k} - \mu_{\mathbf{x}}), \quad (3)$$

where $\sigma_{\mathbf{x}}^2$ and $\mu_{\mathbf{x}}$ are, respectively, the variance and the estimated mean of the components of $\mathbf{x}$, and $k = 0, 1, 2, ..., K$ is a discrete time lag with $K << n$. If $\mu_{\mathbf{x}} = 0$, $C(k)$ is called normalized discrete autocorrelation function.

The covariance matrix $\mathbf{M}$ of $\mathbf{x}$, in its Toeplitz [33, p. 26] form, is computed from (3), leading to

$$\hat{\mathbf{M}} = \begin{bmatrix} C(0) & C(1) & C(2) & \cdots & C(K) \\ C(1) & C(0) & C(1) & \cdots & C(K-1) \\ C(2) & C(1) & C(0) & \cdots & C(K-2) \\ \vdots & \vdots & \vdots & \ddots & \vdots \\ C(K) & C(K-1) & C(K-2) & \cdots & C(0) \end{bmatrix}. \quad (4)$$

In [34] are given several routines related to generation and parameter estimation of αSGN(ξ) samples. Two of them are used herein. The first, named `asgnfit`, returns the estimates of the normalized covariance matrix $\hat{\mathbf{M}}_{\mathrm{n}}$ of the input vector, as well as its parameters α and γ. This routine receives the audio file and the desired memory order ξ as input parameters. From $\hat{\mathbf{M}}_{\mathrm{n}}$, one can calculate [16] the covariance matrix of the audio samples, $\hat{\mathbf{M}}$, which has been found to be

$$\hat{\mathbf{M}} = \gamma^2\hat{\mathbf{M}}_{\mathrm{n}}. \quad (5)$$

It is noteworthy that, according to [34], the estimation of the covariance matrix performed via the `asgnfit` routine is limited to the dimensions $(\xi+1)\times(\xi+1) = 10\times10$.

The impulsivity and scale parameters estimated for the noise generated by the audio file were $\alpha = 1.53$ and $\gamma = 0.0074$, with the corresponding normalized covariance matrix $\hat{\mathbf{M}}_{\mathrm{n}}^{\mathrm{audio}}$ given by

$$\hat{\mathbf{M}}_{\mathrm{n}}^{\mathrm{audio}} = \begin{bmatrix} 1 & 0.639 & 0.035 & -0.167 & -0.065 & -0.055 & -0.140 & -0.168 & -0.177 & -0.200 \\ 0.639 & 1 & 0.639 & 0.035 & -0.167 & -0.065 & -0.055 & -0.140 & -0.168 & -0.177 \\ 0.035 & 0.639 & 1 & 0.639 & 0.035 & -0.167 & -0.065 & -0.055 & -0.140 & -0.168 \\ -0.167 & 0.035 & 0.639 & 1 & 0.639 & 0.035 & -0.167 & -0.065 & -0.055 & -0.140 \\ -0.065 & -0.167 & 0.035 & 0.639 & 1 & 0.639 & 0.035 & -0.167 & -0.065 & -0.055 \\ -0.055 & -0.065 & -0.167 & 0.035 & 0.639 & 1 & 0.639 & 0.035 & -0.167 & -0.065 \\ -0.140 & -0.055 & -0.065 & -0.167 & 0.035 & 0.639 & 1 & 0.639 & 0.035 & -0.167 \\ -0.168 & -0.140 & -0.055 & -0.065 & -0.167 & 0.035 & 0.639 & 1 & 0.639 & 0.035 \\ -0.177 & -0.168 & -0.140 & -0.055 & -0.065 & -0.167 & 0.035 & 0.639 & 1 & 0.639 \\ -0.200 & -0.177 & -0.168 & -0.140 & -0.055 & -0.065 & -0.167 & 0.035 & 0.639 & 1 \end{bmatrix}.$$

The matrix $\hat{\mathbf{M}}_{\mathrm{n}}^{\mathrm{audio}}$ is identical to the one estimated from (3) and (4), which allows to state that the procedure adopted by the routine given in [34] also makes use of (3) and (4).

The other routine from [34] that is explored herein, named `asgn`, generates n samples αSGN(ξ) based on the inputs representing the desired α and covariance matrix. Using $\alpha = 1.53$ and the previously-presented matrix $\hat{\mathbf{M}}_{\mathrm{n}}^{\mathrm{audio}}$ as inputs, the noise αSGN(9) has been generated. With this noise as input to the routine `asgnfit`, the covariance matrix $\hat{\mathbf{M}}_{\mathrm{n}}^{\alpha\mathrm{SGN}(9)}$ has been subsequently estimated. The resulting matrix has been found to be

$$\hat{\mathbf{M}}_{\mathrm{n}}^{\alpha\mathrm{SGN}(9)} = \begin{bmatrix} 1 & 0.648 & 0.046 & -0.179 & -0.092 & -0.063 & -0.127 & -0.158 & -0.184 & -0.218 \\ 0.648 & 1 & 0.648 & 0.046 & -0.179 & -0.092 & -0.063 & -0.127 & -0.158 & -0.184 \\ 0.046 & 0.648 & 1 & 0.648 & 0.046 & -0.179 & -0.092 & -0.063 & -0.127 & -0.158 \\ -0.179 & 0.046 & 0.648 & 1 & 0.648 & 0.046 & -0.179 & -0.092 & -0.063 & -0.127 \\ -0.092 & -0.179 & 0.046 & 0.648 & 1 & 0.648 & 0.046 & -0.179 & -0.092 & -0.063 \\ -0.063 & -0.092 & -0.179 & 0.046 & 0.648 & 1 & 0.648 & 0.046 & -0.179 & -0.092 \\ -0.127 & -0.063 & -0.092 & -0.179 & 0.046 & 0.648 & 1 & 0.648 & 0.046 & -0.179 \\ -0.158 & -0.127 & -0.063 & -0.092 & -0.179 & 0.046 & 0.648 & 1 & 0.648 & 0.046 \\ -0.184 & -0.158 & -0.127 & -0.063 & -0.092 & -0.179 & 0.046 & 0.648 & 1 & 0.648 \\ -0.218 & -0.184 & -0.158 & -0.127 & -0.063 & -0.092 & -0.179 & 0.046 & 0.648 & 1 \end{bmatrix},$$

which is approximately equal to $\hat{\mathbf{M}}_{\mathrm{n}}^{\mathrm{audio}}$, thus validating the correct generation of αSGN(ξ) samples.

To complete the statistical analysis regarding the covariance matrices, SαSN noise samples have been generated via the Matlab's `random` command, using as input the audio-estimated parameters $\alpha = 1.53$ and $\gamma = 0.0074$, $\beta = \delta = 0$, and the number of samples equal to the length of the audio vector. Using the routine `asgnfit` of [34], the estimated covariance matrix $\hat{\mathbf{M}}_{\mathrm{n}}^{\mathrm{S}\alpha\mathrm{SN}}$ has been

$$\hat{\mathbf{M}}_{\mathrm{n}}^{\mathrm{S}\alpha\mathrm{SN}} = \begin{bmatrix} 1 & 0 & -0.001 & 0 & 0 & 0 & 0 & 0 & 0 & 0 \\ 0 & 1 & 0 & -0.001 & 0 & 0 & 0 & 0 & 0 & 0 \\ -0.001 & 0 & 1 & 0 & -0.001 & 0 & 0 & 0 & 0 & 0 \\ 0 & -0.001 & 0 & 1 & 0 & -0.001 & 0 & 0 & 0 & 0 \\ 0 & 0 & -0.001 & 0 & 1 & 0 & -0.001 & 0 & 0 & 0 \\ 0 & 0 & 0 & -0.001 & 0 & 1 & 0 & -0.001 & 0 & 0 \\ 0 & 0 & 0 & 0 & -0.001 & 0 & 1 & 0 & -0.001 & 0 \\ 0 & 0 & 0 & 0 & 0 & -0.001 & 0 & 1 & 0 & -0.001 \\ 0 & 0 & 0 & 0 & 0 & 0 & -0.001 & 0 & 1 & 0 \\ 0 & 0 & 0 & 0 & 0 & 0 & 0 & -0.001 & 0 & 1 \end{bmatrix}.$$

Note that $\hat{\mathbf{M}}_{\mathrm{n}}^{\mathrm{S}\alpha\mathrm{SN}}$ is very close to an identity matrix, which refers to a time series with zero correlation between adjacent samples, as expected when generating SαSN samples via the Matlab's `random` command.

Fig. 1 presents the normalized autocorrelation functions, obtained from (3), for the recorded snapping shrimp noise, for the αSGN(9) noise and for the SαSN noise. Such functions are plotted up to the time lag $k = 20$ for better visualization of the most relevant region, which is located in the vicinity of the discrete-time instant $k = 0$. In the three functions, $C(0) = 1$, since they are normalized with respect to the time-series average power $\sigma_{\mathbf{x}}^2$. As the value of k increases, the autocorrelation decreases, showing that samples further apart are less correlated, as expected. It is verified that there is a close similarity between the values of $C(k)$ for αSGN(9) noise and for audio samples up to $k = 10$. This is an expected outcome, as the dissimilarity is more evident for $k > 10$ due to the fact that the `asgn` routine from [34], which generates the αSGN(ξ), has maximum memory $\xi = 9$, thus limiting the range of the input covariance matrix regarding the representativeness of the entire correlation structure of the reference audio noise. Also as expected, the autocorrelation function of the SαSN samples is practically zero for $k \neq 0$, a consequence of the fact that adjacent samples generated by the Matlab's `random` command are time-uncorrelated. Moreover, it is worth noting that the values of each of the autocorrelation functions shown in Fig. 1 for $k \leq 9$ are equal to the values in the first row of each of the corresponding covariance matrices $\hat{\mathbf{M}}_{\mathrm{n}}^{\mathrm{audio}}$, $\hat{\mathbf{M}}_{\mathrm{n}}^{\alpha\mathrm{SGN}(9)}$ and $\hat{\mathbf{M}}_{\mathrm{n}}^{\mathrm{S}\alpha\mathrm{SN}}$.

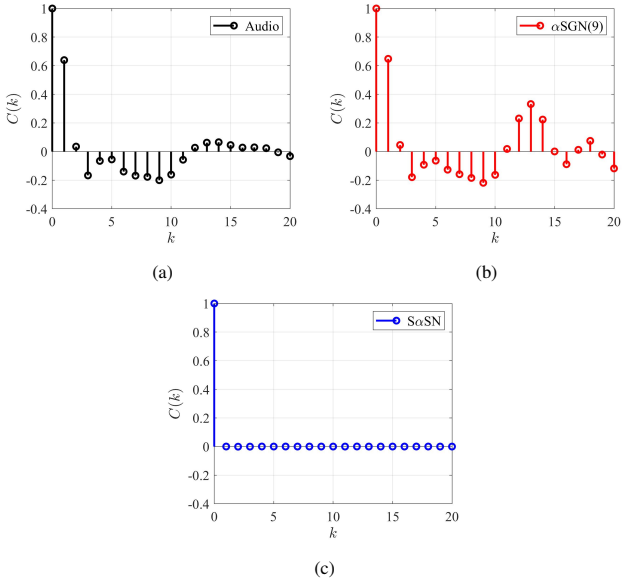

Fig. 1. Normalized discrete autocorrelation function of the snapping shrimp audio samples (a), the αSGN(9) noise (b) and the SαSN noise (c), with a maximum time lag of $k = 20$.

IV. Signals and Systems Models

This section describes the signal model for centralized CSS, the conventional and the DCR-based receiver models, and the test statistics whose performances are analyzed in Section V.

A. Conventional receiver model

In the centralized CSS with data fusion[1], n samples from the signal transmitted by the primary user (PU) are collected by

[1]Alternatively to the centralized CSS with data fusion, there is the centralized CSS with decision fusion, in which local decisions are made in each SU and transmitted to the FC. At the FC, these local decisions are combined to form the global decision on the occupation state of the sensed channel [3].

each of the m cooperating SUs and transmitted to the fusion center (FC) belonging to the secondary network. At the FC, a test statistic is formed through the mn received samples, and its value is compared with a decision threshold in order to decide on the occupation state of the sensed band. In this model, the matrix $\mathbf{Y} \in \mathbb{C}^{m\times n}$ containing the samples received at FC is given by

$$\mathbf{Y} = \mathbf{h}\mathbf{x}^{\mathrm{T}} + \mathbf{V} + \mathbf{W}, \tag{6}$$

where the vector $\mathbf{x} \in \mathbb{C}^{n\times 1}$ that models the PU signal is composed of n complex Gaussian samples with zero mean and variance defined according to the average signal-to-noise ratio (SNR) across the SUs. The adoption of samples with Gaussian distribution matches the behavior of the envelope fluctuations of many modulated and filtered signals. The channel vector $\mathbf{h} \in \mathbb{C}^{m\times 1}$ contains elements h_i, $i = 1, 2, ..., m$, characterizing the gains of the sensing channel between the PU and the i-th SU. This vector is given by

$$\mathbf{h} = \mathbf{G}\mathbf{a}, \tag{7}$$

where $\mathbf{a} \in \mathbb{C}^{m\times 1}$ is a vector formed by complex Gaussian random variables a_i with mean $\sqrt{\kappa/(2\kappa+2)}$ and variance $1/(\kappa+1)$, where κ models the Rice factor of the channel between the PU and each SU. It is assumed that the elements h_i are constant during the sensing interval and independent and identically distributed between consecutive sensing rounds. It is also assumed that the bandwidth of the primary signal is smaller than the coherence bandwidth of the sensing channel, which corresponds to a flat fading channel.

The matrix $\mathbf{G} \in \mathbb{R}^{m\times m}$ in (7) is given by

$$\mathbf{G} = \mathrm{diag}\left(\sqrt{\frac{\mathbf{p}}{p_{\mathrm{avg}}}}\right), \tag{8}$$

where $\mathbf{p} = [p_1 \ p_2 \ \cdots \ p_m]^{\mathrm{T}}$ is the vector with the received signal powers at the SUs and $p_{\mathrm{avg}} = \frac{1}{m}\sum_{i=1}^{m} p_i$. When considering different and time-varying received signal power levels across the SUs, p_i is uniformly distributed in $[(1-\rho_S)p_{\mathrm{avg}}, \ (1+\rho_S)p_{\mathrm{avg}}]$ in each sensing round, where $0 \leq \rho_S < 1$ is a configurable fraction of the received signal power variations around the average.

The matrices $\mathbf{V}$ and $\mathbf{W}$ in (6) account for the noise present in the system, with $\mathbf{V} \in \mathbb{C}^{m\times n}$ representing the AWGN noise and $\mathbf{W} \in \mathbb{C}^{m\times n}$ representing the SαSN or αSGN(ξ) impulsive noise samples. The elements in the i-th row of $\mathbf{V}$ are independent and identically distributed Gaussian random variables, with zero mean and time-varying variance σ_i^2 following a uniform distribution around the mean σ_{avg}^2, in the range $[(1-\rho_N)\sigma_{\mathrm{avg}}^2, \ (1+\rho_N)\sigma_{\mathrm{avg}}^2]$, with $0 \leq \rho_N < 1$ and $\sigma_{\mathrm{avg}}^2 = \frac{1}{m}\sum_{i=1}^{m}\sigma_i^2$.

The SNR, in dB, averaged across the SUs is given by

$$\mathrm{SNR} = 10\log_{10}\left(\frac{p_{\mathrm{avg}}}{\sigma_{\mathrm{avg}}^2}\right). \tag{9}$$

B. Direct-conversion receiver model

The DCR-based CSS model proposed in [13] is grounded on the structure of a typical direct-conversion receiver, whose details were omitted here for brevity. This structure gave rise to the model shown in Fig. 2, which is used as a basis for computer simulations of CSS with data fusion. The model takes into account the main signal processing tasks performed at the SUs' receivers and at the FC, namely: filtering, residual DC-offset addition, automatic gain control, noise whitening, analog-to-digital conversion (quantization), test statistic computation and spectrum occupancy decision.

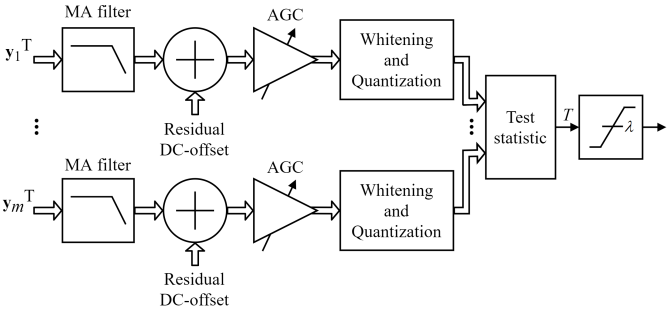

Fig. 2. DCR-based model for CSS with data fusion [13].

The i-th row of the matrix $\mathbf{Y}$, which is denoted by $\mathbf{y}_i^{\mathrm{T}}$, for $i = 1, ..., m$, goes through a moving-average (MA) filter whose impulse response has length L. This filter models all filtering effects on the signals transmitted and received.

The samples in the output of each of the MA filters are added to residual DC-offset samples, modeling the effect of the residual direct-current (DC) delivered by typical DC-offset compensation strategies. As the name suggests, the DC-offset is a DC value added to the desired signal primarily due to local-oscillator self-mixing and in-band interfering signals [12]. The variance of the DC-offset samples, σ_{dc}^2, is determined according to the signal-to-DC-offset ratio (SDCR), whose value, in dB, is given by

$$\mathrm{SDCR} = 10\log_{10}\left(\frac{p_{\mathrm{avg}}}{\sigma_{\mathrm{dc}}^2}\right). \tag{10}$$

The automatic gain control (AGC) combines the amplification stages promoted by the receiver. In the i-th SU, $i = 1, 2, ..., m$, the gain is defined as

$$g_i = \frac{f_{\mathrm{od}}\sqrt{2n}}{6\|\mathbf{y}_i\|}, \tag{11}$$

where $\|\cdot\|$ represents the Euclidean norm and f_{od} is the overdrive factor that models the different signal clipping levels present in real analog-to-digital converters (ADCs).

The samples corrupted by DC-offset are then digitized before noise whitening [35], a step that aims to reduce the degree of correlation induced by filtering effects at the transmitter, at the channel and at the input of the receiver. Noise whitening is sensitive to low resolution and needs to be done under high resolution. After that, the already whitened samples undergo a new quantization process with low resolution for data transmission to the FC, thus occupying a smaller bandwidth in the control channel used for such a transmission; an error-free control channel is considered herein. In practice, it might be convenient to perform noise whitening at the FC to alleviate

the processing burden at the SUs. The present model applies in both localizations of whitening.

Inside the 'Whitening and Quantization' block shown in Fig. 2, the whitening filter [35] matrix $\mathbf{B} \in \mathbb{R}^{n\times n}$ that multiplies the version of $\mathbf{Y}$, which has been modified by the AGC and quantization, is given by

$$\mathbf{B} = \mathbf{U}\mathbf{L}^{-1}, \tag{12}$$

where $\mathbf{U}$ is an orthogonal arbitrary matrix obtained by singular value decomposition of the covariance matrix $\mathbf{Q} \in \mathbb{R}^{n\times n}$, which is associated with the impulse response of the MA filter. The elements of $\mathbf{Q}$ are

$$Q_{ij} = q_{|i-j|}, \tag{13}$$

for $i, j = 1, 2, ..., n$, with q_k denoting the discrete auto-correlation function of the MA filter impulse response, i.e., $q_k = 1 - k/L$ for $k \leq L$, and $q_k = 0$ otherwise, for $k = 0, 1, ..., (n-1)$. The matrix $\mathbf{L}$ in (12) is the lower triangular matrix obtained from the Cholesky decomposition of $\mathbf{Q}$. The desired power levels are ensured by setting the impulse response of the MA filter to $z_l = 1/\sqrt{L}$ for $l = 1, ..., L$.

C. Test statistics

Spectrum sensing corresponds to a binary hypothesis test in which the null hypothesis $\mathcal{H}_0$ is associated with the absence of the primary signal in the sensed band and the alternative hypothesis $\mathcal{H}_1$ is associated with the presence of the primary signal. The test is performed by comparing a test statistic T with a decision threshold λ. If $T > \lambda$, the hypothesis $\mathcal{H}_0$ is rejected. Otherwise, $\mathcal{H}_0$ is accepted.

Hereafter, in terms of the DCR model shown in Fig. 2, the elements of $\mathbf{Y}$ are those obtained after MA filtering, DC-offset addition, AGC, whitening and quantization. If the conventional model is adopted, $\mathbf{Y}$ contains the received samples free from any hardware-related signal processing.

The ED test statistic, considering centralized CSS with data fusion in the conventional model, is given by [3]

$$T_{\mathrm{ED}} = \sum_{i=1}^{m} \frac{1}{\sigma_i^2} \sum_{j=1}^{n} |y_{ij}|^2, \tag{14}$$

where σ_i^2 is the Gaussian noise variance at the i-th SU and y_{ij} denotes the j-th sample collected by the i-th SU, which composes the matrix $\mathbf{Y}$ defined in (6).

Considering the DCR, the ED test statistic becomes

$$T_{\mathrm{ED}_{\mathrm{dcr}}} = \sum_{i=1}^{m} \frac{1}{g_i^2\sigma_i^2} \sum_{j=1}^{n} |y_{ij}|^2, \tag{15}$$

where g_i is the variable corresponding to the composition of gains established by the AGC in the i-th SU [13], as defined in (11).

The test statistic of the AVC detector [36], [37], which is formed at the FC in the case of centralized CSS with data fusion, in the conventional model is given by

$$T_{\mathrm{AVC}} = \sum_{i=1}^{m} \frac{1}{\sigma_i} \sum_{j=1}^{n} |y_{ij}|. \tag{16}$$

Considering the DCR-based spectrum sensor model, the AVC test statistic becomes

$$T_{\mathrm{AVC}_{\mathrm{dcr}}} = \sum_{i=1}^{m} \frac{1}{g_i\sigma_i} \sum_{j=1}^{n} |y_{ij}|. \tag{17}$$

The other test statistics considered hereafter are built from the sample covariance matrix (SCM) of the received signal, which is computed at the FC[2] as

$$\hat{\mathbf{R}} = \frac{1}{n}\mathbf{Y}\mathbf{Y}^{\dagger}, \tag{18}$$

where † denotes complex conjugate and transpose.

The test statistic of the GRCR detector [38] is given by

$$T_{\mathrm{GRCR}} = \frac{\sum_{i=1}^{m} \sum_{j=1, j\neq i}^{m} |r_{ij}|}{\sum_{i=1}^{m} r_{ii}}, \tag{19}$$

where r_{ij} is the element in the i-th row and j-th column of the SCM matrix, $\hat{\mathbf{R}}$.

The test statistics of the GID [39] and PRIDe [40] detectors are given respectively by

$$T_{\mathrm{GID}} = \frac{\sum_{i=1}^{m^2} |r_i|}{\sum_{i=1}^{m^2} \sum_{j=1}^{m^2} |r_i - r_j|} \tag{20}$$

and

$$T_{\mathrm{PRIDe}} = \frac{\sum_{i=1}^{m^2} |r_i|}{\sum_{i=1}^{m^2} |r_i - \bar{r}|}, \tag{21}$$

where r_i is the i-th element of the vector $\mathbf{r}$ formed by stacking the columns of $\hat{\mathbf{R}}$ and $\bar{r} = (1/m^2)\sum_{i=1}^{m^2} r_i$.

For the LMPIT [41] detector, the test statistic is

$$T_{\mathrm{LMPIT}} = \sum_{i=1}^{m} \sum_{j=1}^{m} |c_{ij}|^2, \tag{22}$$

where c_{ij} is the element in the i-th row and j-th column of the matrix $\mathbf{C} = \mathbf{E}^{-1/2}\hat{\mathbf{R}}\mathbf{E}^{-1/2}$, with $\mathbf{E}$ being a diagonal matrix whose elements are equal to the main diagonal of the SCM.

According to [13], the GRCR, GID, PRIDe and LMPIT detectors have low computational complexity. They are also blind, in the sense that no information is needed about the PU signal, nor the noise variance. The ED and the AVC are semi-blind, since they require no information about the PU signal, but make use of the noise level information (respectively the noise variance and its standard deviation). The GRCR, GID, PRIDe and LMPIT detectors are also considered robust

[2]In terms of the DCR model shown in Fig. 2, the SCM is computed inside the block 'Test Statistic', if the detector is based on the SCM.

detectors because they attains little or no change in their performances with the temporal variation of the noise variance, the received signal power or both [3].

V. Spectrum sensing performance results

This section presents computer simulation results of the centralized CSS with data fusion. Conventional and DCR-based receiver models are compared, in the absence and presence of impulsive noise, for the detectors ED, AVC, GRCR, GID, PRIDe and LMPIT.

Spectrum sensing performance is often measured by means of the probability of detection, $P_{\rm d}$, and the probability of false alarm, $P_{\rm fa}$ [3]. $P_{\rm d}$ is the probability of deciding that the primary signal is present in the sensed band, when it is actually present, whereas $P_{\rm fa}$ is the probability of deciding that such a signal is present, when it is, in fact, absent.

The results reported in this section give, for each of the above-mentioned test statistics, the values of $P_{\rm d}$ obtained according to the variation of the most relevant system parameters, assuming $P_{\rm fa} = 0.1$ [42]. Each point on a curve has been generated from 10000 Monte Carlo events, which corresponds to the generation of the same number of each test statistic under the hypotheses $\mathcal{H}_0$ and $\mathcal{H}_1$. Following [13], a confidence interval analysis has been carried out by means of the binomial proportion confidence interval for single proportion, using the Matlab function `binofit`, which adopts the Clopper-Pearson method [43]. The maximum confidence interval, which is associated to an estimate of $P_{\rm d}$ equal to 0.5, is 0.0197, conferring adequate accuracy to the analyses of the results presented herein. The Matlab code used to generate these results can be retrieved from [44].

Taking the conventional receiver as the reference in the absence of impulsive noise, the value of the average SNR or the number of samples, n, has been adjusted, in some cases, so that the best detector yields $P_{\rm d} \approx 0.9$ at the mid-value of the system parameter being analyzed. By doing so, the variations caused in $P_{\rm d}$ by the values below or above this mid-value can be easily analyzed. When fixed, the system parameters are: $m = 6$ SUs, $n = 140$ samples, SNR $= -10$ dB, SDCR $= 5$ dB, $N_{\rm q} = 8$ quantization levels (3 bits), overdrive factor $f_{\rm od} = 1.2$, filter impulse response length $L = n/10$, fractions of signal and noise variations $\rho_S = 0.9$ and $\rho_N = 0.45$, respectively, and Rice factor $\kappa = 3$ dB [45].

The parameters related to the impulsive noise have been estimated as described in Section III. The value of the characteristic exponent has been kept fixed as $\alpha = 1.53$, whereas the scale factor has been adjusted to $\gamma = 0.15$, so that the influence of impulsive noise in the spectrum sensing performance is clearly perceived in the graphs.

Figs. 3 to 9 shows $P_{\rm d}$ as a function of the following system configuration parameters: number of secondary users, m; number of samples collected by each SU during each sensing interval, n; average signal-to-noise ratio, SNR; overdrive factor, $f_{\rm od}$; signal-to-DC-offset ratio, SDCR; MA filter impulse response length, L, and number of quantization bits, $\log_2 N_{\rm q}$, with $N_{\rm q}$ being the number of quantization levels. Figs. 3 to 5 each have three pairs of graphs assuming the absence and presence of impulsive noise, whether SαSN or αSGN(9). Each pair gives performance results of the detectors when the conventional receiver model (on the left) or the DCR model (on the right) is adopted. Figs. 6 to 9 show $P_{\rm d}$ as a function of parameters present exclusively in the DCR model.

Before any further interpretations of the results are presented, it is important to highlight that a given detector does not have its performance influenced in the same way as another detector for the same system setting and the same variation of a given parameter, since the received signal samples are processed in different ways by the test statistics, thus resulting in different behaviors among the detectors.

Fig. 3 gives $P_{\rm d}$ versus m. In the conventional receiver model (left-hand side graphs), it can be seen, as expected, that $P_{\rm d}$ increases with an increase in m, but in different proportions for the different detectors. This is justified by the directly proportional relationship between the spatial diversity gain and the number of SUs in cooperation. The ED achieves useless performance when submitted to both impulsive noise types. The AVC do the same when impaired by αSGN(9). When the DCR model is considered (right-hand side graphs), the patterns of the curves are similar to that of the conventional model (on the left), except for the AVC, whose performance in the presence of SαSN is also useless. It is noteworthy that impulsive noise introduces a performance loss in all detectors when compared under the same receiver model in the absence of impulsive noise.

Fig. 3a, which corresponds to the absence of impulsive noise, is in accordance with the results reported in [13], thus serving also as a validation of the simulations used herein. It can be noticed the performance worsening for all detectors from the conventional to the DCR model. Notice that the worsening is more pronounced for the detectors AVC and ED.

From Figs. 3b and 3c, which consider impulsive noise, it can be seen that the performances of the GID, PRIDe and GRCR have suffered less reduction under the DCR model than under the conventional receiver model for both impulsive noise types, taking the absence of impulsive noise as reference, whereas the opposite occurred with the LMPIT, and with the AVC under SαSN. The ED has been maintained useless when impaired by any of the impulsive noise types. There is also a change in the performance rating of the detectors, from the conventional to the DCR model. In both models, the AVC and the ED unveiled significant sensitivity to impulsive noise, with the former slightly outperforming the latter in the conventional model, under SαSN. The GID and PRIDe, on the other hand, deserve special attention as they yielded, in the most realistic scenario in which the DCR model is used, greater robustness against impulsive noise.

The effects on $P_{\rm d}$ when n is varied are shown in Fig. 4. As expected, for the conventional (left) and DCR (right) models, most detectors, even if in different proportions, showed an improvement in performance with the increase of n. This is justified due to the greater amount of samples collected by each SU, in a given sensing interval, for a fixed sampling rate, enhancing the accuracy in the decision by the occupation state of the licensed band. Again, in the conventional model, the exception is in the performance of the ED, under both im-

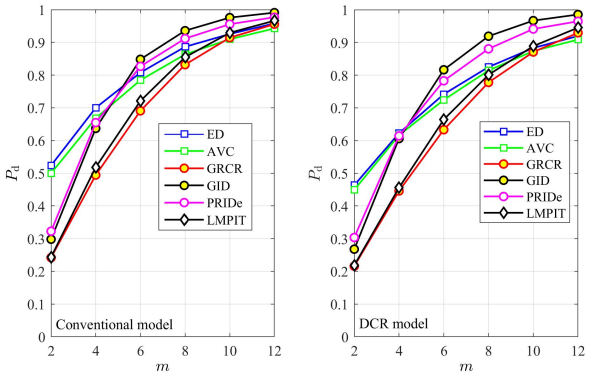

(a) Absence of impulsive noise.

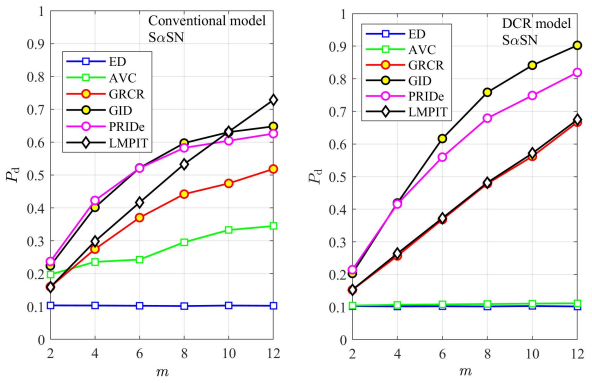

(b) Presence of SαSN.

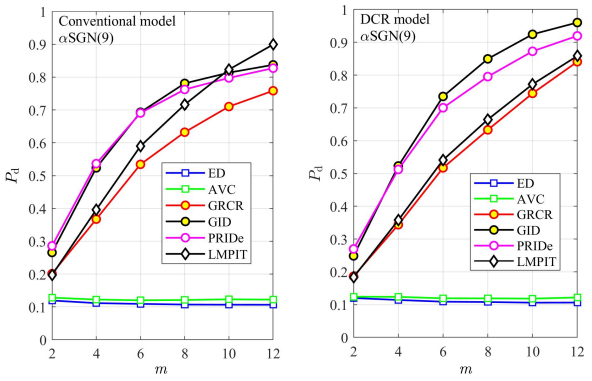

(c) Presence of αSGN(9).

Fig. 3. Probability of detection, P_d, versus number of SUs, m, for SNR $= -10.75$ dB: conventional model (left), DCR model (right). This figure is better viewed in color.

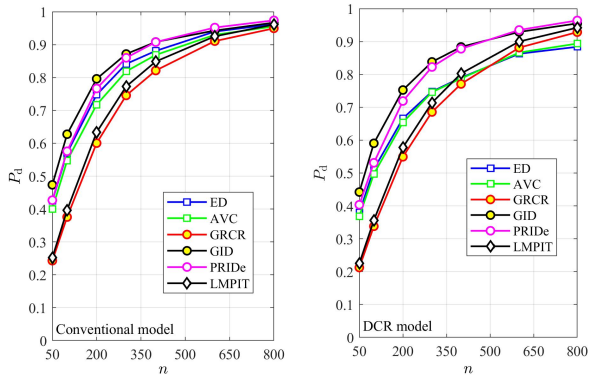

(a) Absence of impulsive noise.

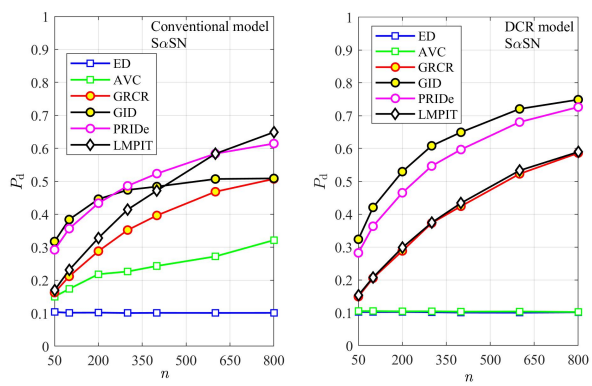

(b) Presence of SαSN.

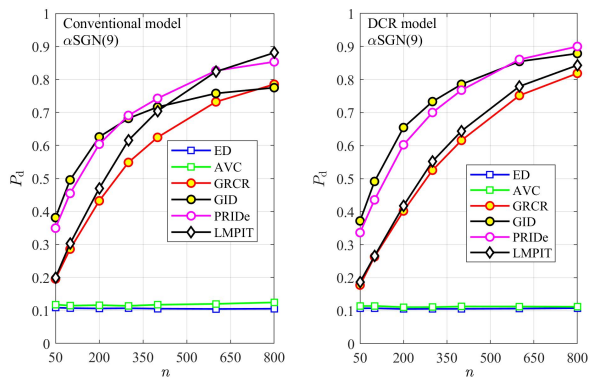

(c) Presence of αSGN(9).

Fig. 4. Probability of detection, P_d, versus number of samples, n, for SNR $= -12.25$ dB: conventional model (left), DCR model (right). This figure is better viewed in color.

pulsive noises, and of the AVC, under αSGN(9). Such curves remained invariant with the variation of n. This behavior is repeated in the DCR model for the performance of the ED and AVC detectors submitted to both SαSN and αSGN(9).

Fig. 4a shows the expected performance degradation from the conventional to the DCR-based receiver model in the absence of impulsive noise, which is in agreement with Fig. 3a and [13].

When impulsive noise is present, as depicted in Figs. 4b and 4c, the GID, PRIDe and GRCR detectors attained a less pronounced performance degradation under the DCR model (right) than in the case of the conventional model, taking the conventional model without impulsive noise as the reference. The LMPIT, in this same aspect, suffered more severe degradation. Again, in the more realistic scenario in which the DCR model is used, the GID and PRIDe detectors stand out for being quite robust to impulsive noise. On the other hand, the ED and the AVC unveiled, once again, poor performance in the presence of impulsive noise, both in the conventional and in the DCR models.

The results depicted in Fig. 5 show that P_d increases with the SNR, as expected, unless the robustness of a detector against impulsive noise is poor to the point of preventing or diminishing the notability of this behavior.

From Fig. 5 it can be also seen that, when the conventional model is considered (left-hand graphs), the AVC and the ED are quite sensitive to impulsive noise, with the former mildly outperforming the latter in presence of αSGN(9), and

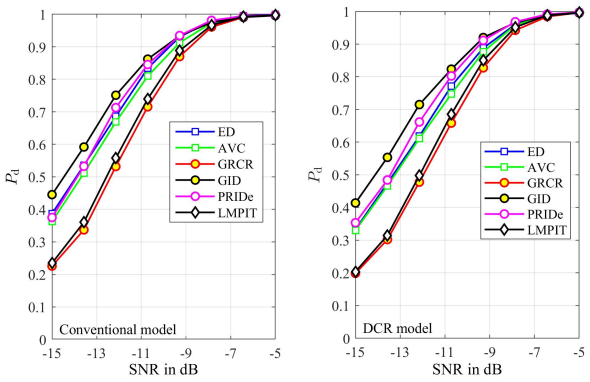

(a) Absence of impulsive noise.

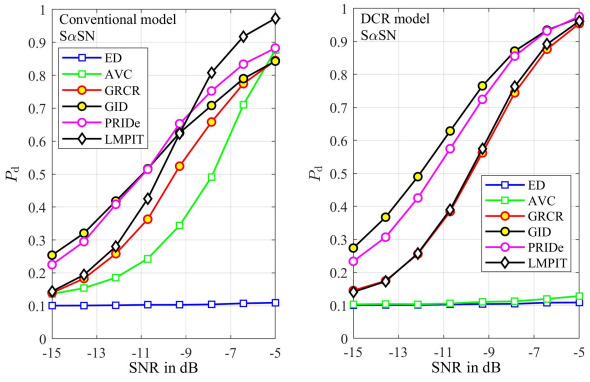

(b) Presence of SαSN.

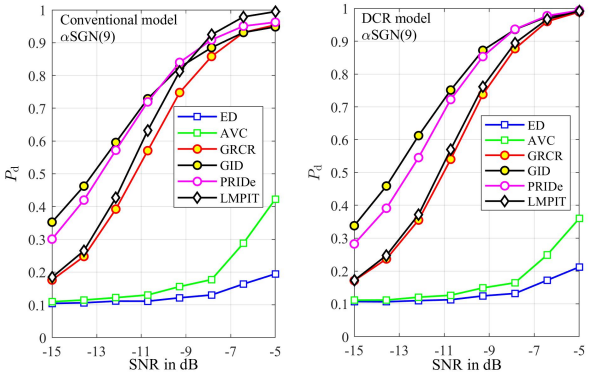

(c) Presence of αSGN(9).

Fig. 5. Probability of detection, P_{d}, versus average SNR for $n = 150$: conventional model (left), DCR model (right). This figure is better viewed in color.

outperforming more noticeably when the SαSN is present. When the DCR model is adopted (right), these detectors are still sensitive to impulsive noise, but there is no significant performance difference between them.

In Fig. 5a, as already reported in [13], and in Figs. 3a and 4a, it can be verified the degradation imposed by the DCR model with respect to the conventional. In Figs. 5b and 5c, when the DCR model (right) is compared with the conventional model (left), it is observed a lower sensitivity to impulsive noise for the detectors GID, PRIDe and GRCR, as well as a greater sensitivity of the LMPIT, in this same condition, in relation to the absence of impulsive noise. The SαSN causes a significant performance loss in the AVC under the DCR model with respect to the conventional, without impulsive noise, whereas this loss is less pronounced when the αSGN(9) is present. Again, the GID and PRIDe detectors stood out from the others in the most realistic situation corresponding to the use of DCR-based model, whereas the AVC and the ED proved to have low robustness against impulsive noise.

Fig. 6 shows a negligible performance variation of all detectors as the overdrive factor, f_{od}, is changed. They all exhibit curves with a certain concavity. For smaller values of f_{od}, the signal excursion is smaller than the dynamic range of the ADC, causing a performance reduction due to the fact that such signal crosses a smaller number of quantization levels. For large values of f_{od}, there is the possibility of strong signal clipping, thus reducing the performance.

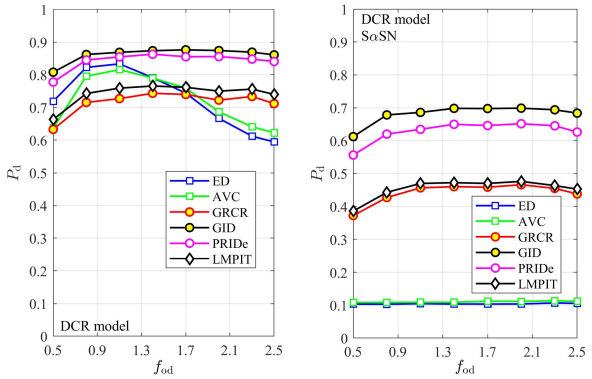

(a) Absence of impulsive noise. (b) Presence of SαSN.

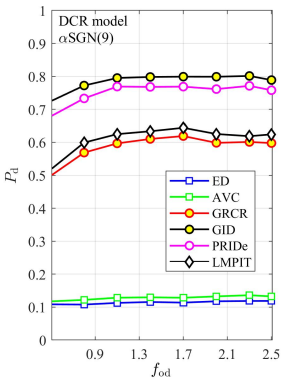

(c) Presence of αSGN(9).

Fig. 6. Probability of detection, P_{d}, versus overdrive factor, f_{od}: DCR model. This figure is better viewed in color.

For the DCR model, one can see, in Fig. 6a, an anomalous behavior in the ED and AVC curves, in the absence of impulsive noise. This is because quantization also affects the noise variance information used to compute both test statistics, which portrays another form of performance loss in addition to those that are caused by lower and higher values of f_{od}.

Figs. 6b and 6c show that there is a smaller performance loss of the GID and PRIDe detectors, in comparison to absence of impulsive noise, becoming more accentuated under SαSN than under αSGN(9). On the other hand, the LMPIT and GRCR detectors attained a slightly more accentuated loss under both impulsive noise models. Once again, the ED and the AVC proved to be significantly sensitive to impulsive noise in the most realistic scenario that adopts the DCR model, while the GID and the PRIDe showed evident robustness in this scenario.

Fig. 7 gives P_{d} versus the SDCR. As expected, lower values of SDCR return worse performances. In general, for most of the detectors in analysis, the increase of P_{d} with the SDCR occurs up to ≈ -5 dB. Beyond this value, P_{d} remains approximately invariant, indicating that the corresponding residual DC-offset is not capable of causing performance degradation.

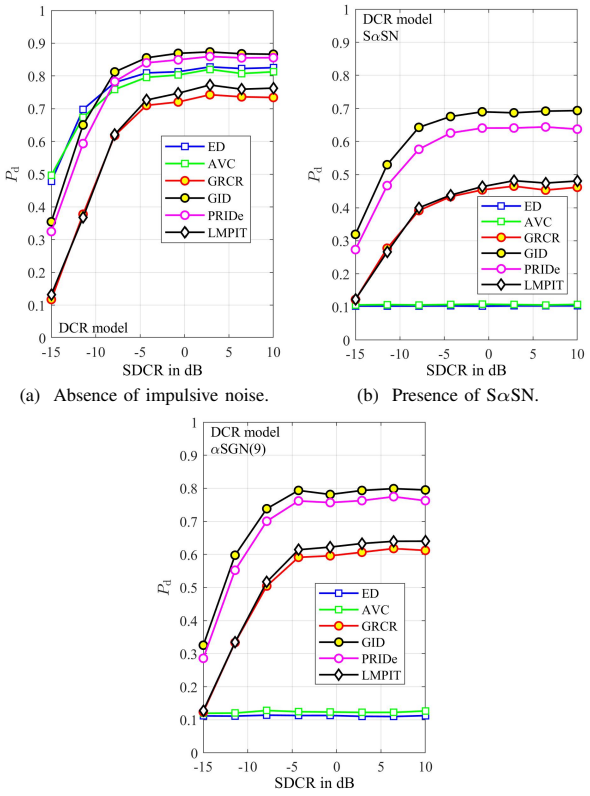

(a) Absence of impulsive noise. (b) Presence of SαSN.

(c) Presence of αSGN(9).

Fig. 7. Probability of detection, P_{d}, versus average SDCR: DCR model. This figure is better viewed in color.

It is also observed in Figs. 7b and 7c that, under impulsive noise, there is less evident performance deterioration of the GID and PRIDe detectors, with a higher sensitivity of the LMPIT and the GRCR. The GID attains a superior performance, followed respectively by the PRIDe, the LMPIT and the GRCR. When impaired by SαSN and αSGN(9), the ED and the AVC are considerably prone to impulsive noise, attaining the worst performances when compared to the scenario without impulsive noise.

Fig. 8 shows how P_{d} is influenced by the resolution (number of bits, $\log_2 N_{\mathrm{q}}$) adopted to digitize the samples transmitted from the SUs to the FC. As expected, the performances of all detectors improve with the increase of this resolution. It can be also seen in all graphs of Fig. 8 that the spectrum sensing performance practically does not improve beyond a 3-bit resolution, meaning that eight quantization levels are enough to represent the samples sent to the FC, a result that is consistent with [12].

Fig. 8a, which considers the absence of impulsive noise, shows the AVC and the ED with the poorest performances for 1-bit resolution, but overcoming the LMPIT and the GRCR above 3 bits. The GID and the PRIDe perform better than the

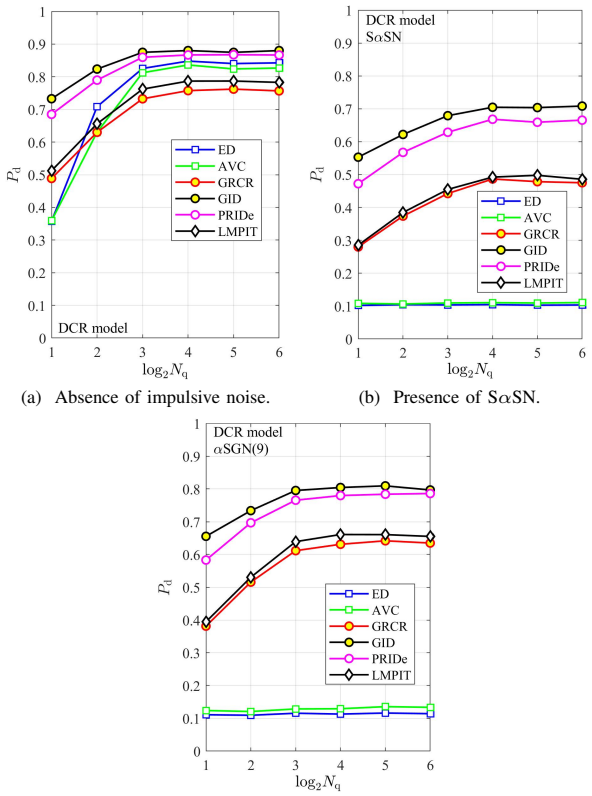

(a) Absence of impulsive noise. (b) Presence of SαSN.

(c) Presence of αSGN(9).

Fig. 8. Probability of detection, P_{d}, versus number of quantization bits, $\log_2 N_{\mathrm{q}}$: DCR model. This figure is better viewed in color.

others for any number of quantization bits.

From Figs. 8b and 8c, it can be seen that the patterns of the curves of the GID, PRIDe, LMPIT and GRCR performances, is repeated in the presence of SαSN and αSGN(9), except for the less accentuated worsening caused by αSGN(9), in all detectors, in comparison to the absence of impulsive noise. The ED and the AVC unveiled a similar behavior, that is, they returned the worst performances under SαSN and αSGN(9).

The effects of the impulse response length L of the MA filter on P_{d} are shown in Fig. 9. There is a mild performance decrease with the increase of L for the GID, PRIDe, LMPIT and GRCR detectors, and a little more accentuated performance decrease for the ED and for the AVC at higher values of L, in the absence of impulsive noise, as shown in Fig. 9a. The higher the value of L, the higher becomes the temporal correlation between adjacent signal samples, which makes the whitening process to become unable to fully restore the decorrelation, which in turn compromises the spectrum sensing performance.

As can be seen in Figs. 9b and 9c, the ED and the AVC again achieve the worst performances when impaired by impulsive noise. And once again, a less accentuated performance worsening is being caused by the αSGN(9) for all detectors, when compared to that caused by the SαSN, taking the absence of impulsive noise as the reference. The GID and the PRIDe deserve special attention once again, because they unveiled significant robustness against impulsive noise in the most realistic situation that considers the use of a DCR.

Finally, based on the statistical analyses of the impulsive

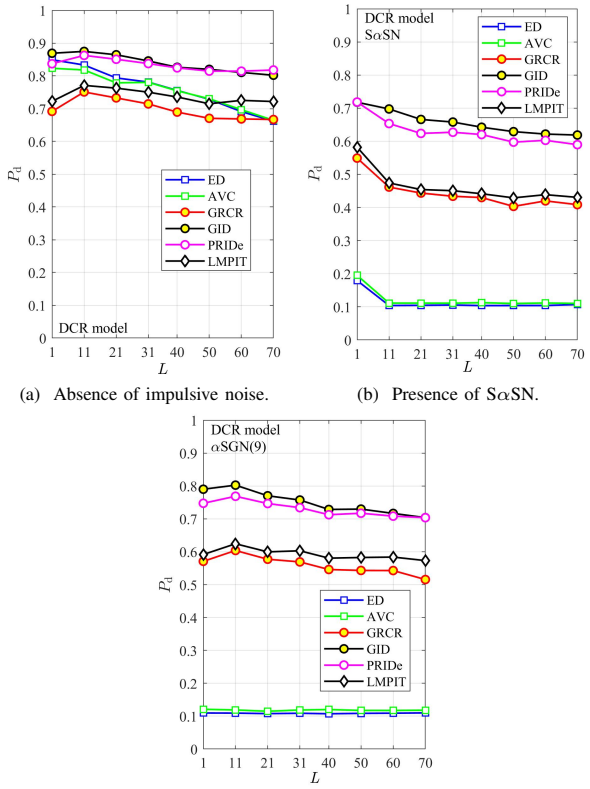

(a) Absence of impulsive noise. (b) Presence of SαSN.

(c) Presence of αSGN(9).

Fig. 9. Probability of detection, P_d, versus impulse response length of the MA filter, L: DCR model. This figure is better viewed in color.

noise models and on the spectrum sensing performance assessment, it has been found that the αSG distribution better suits to model the snapping shrimp impulsive noise than the SαS distribution. However, the main disadvantage of the algorithm described in [34] to generate αSGN(9) samples is its high computational burden. This is illustrated in Fig. 10, which shows the time spent to generate SαSN and αSGN(9) noise samples. The SαSN samples have been generated using the Matlab's `random` function and the time measurements has been made via the Matlab's `tic-toc` function. For example, for $n = 5000$ samples, the time spent by the αSGN(9) generator is ≈ 100 times larger than in the case of the SαSN generator. Fig. 10 has been constructed using a computer with the Intel Core i5-4210U CPU @ 1.70 GHz, with 8 GB of RAM, running Matlab version R2019a.

VI. Conclusions

This work has assessed the performance of centralized cooperative spectrum sensing with data fusion, under symmetric α-stable and α-sub-Gaussian impulsive noises, using a conventional and a direct-conversion sensor receiver model. The performances of the detectors ED, AVC, GRCR, GID, PRIDe and LMPIT were compared under different receiver and noise models, in the context of underwater acoustic communications.

The suitability of the SαS and αSG distributions has been addressed to model the snapping shrimp impulsive noise, a form of noise that can affect the performance of underwater spectrum sensing. Results revealed that there is a correlation

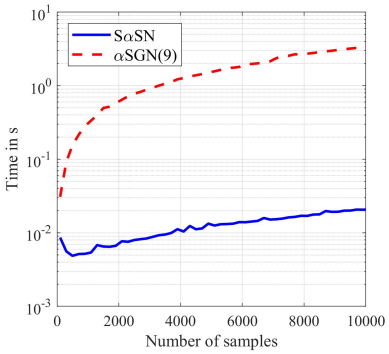

Fig. 10. Time spent (in seconds) to generate SαSN and αSGN(9) samples.

among the samples of the real snapping shrimp noise, which can be adequately modeled by the αSG distribution. The SαS distribution, although adequately models the amplitude variations of the snapping shrimp noise, does not take into account the temporal correlation between adjacent noise samples.

Although there is a great adherence between a real snapping shrimp noise and αSGN samples, the time required to generate SαSN samples is significantly smaller than in the case of αSGN samples.

The DCR model, in the absence of impulsive noise, introduces degradation in the performance of all detectors when compared to the conventional model. The ED and the AVC have showed a more accentuated degradation due to the received signal processing steps considered in the DCR and its influences in the computation of both test statistics. The LMPIT and GRCR detectors have showed a similar behavior, with the former slightly outperforming the latter according to the variation of all parameters using the DCR model.

In the presence of impulsive noise, the results showed that not modeling the temporal correlation causes the performance to be underestimated for most of the detectors analyzed, whether in the conventional or the DCR model.

As for the specific parameters of the DCR model, even in the presence of impulsive noise, the signal-to-DC-offset ratio and the number of quantization levels have produced quite significant spectrum sensing performance variations, when compared to the other parameters. For most of the detectors, three quantization bits are sufficient to represent the digitized samples to be transmitted from the SUs to the FC.

We highlight that the ED and the AVC unveiled low robustness against impulsive noise for any variations of the parameters that are part of the DCR model.

The detectors GID and PRIDe have been highlighted from the other ones, as they have yielded, in the most realistic scenario in which the DCR model is used, greater robustness against impulsive noise. This is an indication that actual implementations of these detectors can result in spectrum sensors very robust against impulsive noise.

Given the large computational burden of the routine used to generate αSGN samples, it is an interesting research opportunity to develop an alternative routine, aiming at a reduced processing time.

The assessment of other detectors for spectrum sensing adopting the models and procedures described herein also

represents an opportunity for contributions.

The hardware implementation of a detector, especially the GID and the PRIDe, can be used to validate the DCR-based model and bring new insights and conclusions from an even more practical standpoint.

ACKNOWLEDGEMENTS

To the Captain-of-Sea-and-War RM1-T, M. V. da S. Simões, Submarine Acoustic Group, Brazilian Navy, ref. Official Letter No. 239/IEAPM-MB, and to Prof. Dr. J. S. G. Panaro, Federal Fluminense University (UFF-RJ), for providing the recorded audio files of the snapping shrimp noise.

REFERENCES

[1] A. Osseiran, F. Boccardi, V. Braun, K. Kusume, P. Marsch, M. Maternia, O. Queseth, M. Schellmann, H. Schotten, H. Taoka, H. Tullberg, M. A. Uusitalo, B. Timus, and M. Fallgren, "Scenarios for 5G mobile and wireless communications: The vision of the METIS project," *IEEE Communications Magazine*, vol. 52, no. 5, pp. 26–35, May 2014, doi: 10.1109/MCOM.2014.6815890.

[2] Y. Arjoune and N. Kaabouch, "A comprehensive survey on spectrum sensing in cognitive radio networks: Recent advances, new challenges, and future research directions," *Sensors*, vol. 19, no. 1, 2019, doi: 10.3390/s19010126.

[3] D. A. Guimarães, "Spectrum sensing: A tutorial," *Journal of Communication and Information Systems*, vol. 37, no. 1, pp. 10–29, Feb. 2022, doi: 10.14209/jcis.2022.2.

[4] B. Mishachandar and S. Vairamuthu, "An underwater cognitive acoustic network strategy for efficient spectrum utilization," *Applied Acoustics*, vol. 175, Apr. 2021, doi: 10.1016/j.apacoust.2020.107861.

[5] Y. Luo, L. Pu, M. Zuba, Z. Peng, and J. Cui, "Challenges and opportunities of underwater cognitive acoustic networks," *Emerging Topics in Computing, IEEE Transactions on*, vol. 2, pp. 198–211, June 2014, doi: 10.1109/TETC.2014.2310457.

[6] A. Wang, B. Li, and Y. Zhang, "Underwater acoustic channels characterization for underwater cognitive acoustic networks," in *2018 International Conference on Intelligent Transportation, Big Data and Smart City (ICITBS)*, 2018, pp. 223–226, doi: 10.1109/ICITBS.2018.00065.

[7] J. Quintas, R. Petroccia, A. Pascoal, J. Cruz, P. Gois, L. Morlando, and M. Stipanov, "Hybrid acoustic-optical underwater communication networks for next-generation cooperative systems: the eumr experience," in *OCEANS 2021: San Diego – Porto*, 2021, pp. 1–7, doi: 10.23919/OCEANS44145.2021.9706085.

[8] Y. Su, T. Zhang, Z. Jin, and L. Guo, "An anti-attack trust mechanism based on collaborative spectrum sensing for underwater acoustic sensor networks," in *Global Oceans 2020: Singapore – U.S. Gulf Coast*, 2020, pp. 1–5, doi: 10.1109/IEEECONF38699.2020.9389150.

[9] T. Shongwe, A. J. H. Vinck, and H. C. Ferreira, "A study on impulse noise and its models," *SAIEE Africa Research Journal*, vol. 106, no. 3, pp. 119–131, 2015, doi: 10.23919/SAIEE.2015.8531938.

[10] X. Liu, L. Du, and S. Xu, "GLRT-based coherent detection in sub-gaussian symmetric alpha-stable clutter," *IEEE Geoscience and Remote Sensing Letters*, vol. 19, pp. 1–5, 2022, doi: 10.1109/LGRS.2021.3094847.

[11] B. Razavi, "Design considerations for direct-conversion receivers," *IEEE Transactions on Circuits and Systems II: Analog and Digital Signal Processing*, vol. 44, no. 6, pp. 428–435, 1997, doi: 10.1109/82.592569.

[12] D. A. Guimarães and R. A. A. de Souza, "Implementation-oriented model for centralized data-fusion cooperative spectrum sensing," *IEEE Communications Letters*, vol. 16, no. 11, pp. 1804–1807, 2012, doi: 10.1109/LCOMM.2012.092112.121614.

[13] D. A. Guimarães and E. J. T. Pereira, "Influence of a direct-conversion receiver model on the performance of detectors for spectrum sensing," *Journal of Communication and Information Systems*, vol. 36, no. 1, p. 173–183, Nov. 2021, doi: 10.14209/jcis.2021.19.

[14] P. Georgiou, P. Tsakalides, and C. Kyriakakis, "Alpha-stable modeling of noise and robust time-delay estimation in the presence of impulsive noise," *IEEE Transactions on Multimedia*, vol. 1, no. 3, pp. 291–301, 1999, doi: 10.1109/6046.784467.

[15] A. Mahmood and M. Chitre, "Modeling colored impulsive noise by Markov chains and alpha-stable processes," in *OCEANS 2015 - Genova*, 2015, pp. 1–7, doi: 10.1109/OCEANS-Genova.2015.7271550.

[16] ——, "Optimal and near-optimal detection in bursty impulsive noise," *IEEE Journal of Oceanic Engineering*, vol. 42, no. 3, pp. 639–653, 2017, doi: 10.1109/JOE.2016.2603790.

[17] L. G. B. Guedes and D. A. Guimarães, "Análise das distribuições SαS e αSG na modelagem do ruído de camarão-de-estalo," in *XL Simpósio Brasileiro de Telecomunicações e Processamento de Sinais (SBrT 2022)*, Santa Rita do Sapucaí, MG, Brazil, Sep. 2022, doi: 10.14209/sbrt.2022.1570823103.

[18] J. V. M. Cardoso, W. J. L. Queiroz, H. Liu, and M. S. Alencar, "On the performance of the energy detector subject to impulsive noise in κ — μ, α — μ, and η — μ fading channels," *Tsinghua Science and Technology*, vol. 22, no. 4, pp. 360–367, 2017, doi: 10.23919/TST.2017.7986939.

[19] H. Qu, X. Xu, J. Zhao, F. Yan, and W. Wang, "A robust hyperbolic tangent-based energy detector with Gaussian and non-Gaussian noise environments in cognitive radio system," *IEEE Systems Journal*, vol. 14, no. 3, pp. 3161–3172, 2020, doi: 10.1109/JSYST.2019.2959045.

[20] H. E. Adardour and S. Kameche, "Identify the primary signal buried under impulsive noise channel in cognitive radio networks using MAF-KF-NPD," in *2018 International Conference on Applied Smart Systems (ICASS)*, 2018, pp. 1–6, doi: 10.1109/ICASS.2018.8652081.

[21] P. H. C. de Souza, D. A. Guimarães, and G. P. Aquino, "Efficient fusion of spectrum sensing information under parameter uncertainty and impulsive noise," *Journal of Communication and Information Systems*, vol. 33, no. 1, Apr. 2018, doi: 10.14209/jcis.2018.5.

[22] A. Halaki, C. Manohar, S. Gurugopinath, and R. Muralishankar, "Entropy-based spectrum sensing under symmetric alpha stable impulsive noise," in *2019 International Conference on Wireless Communications Signal Processing and Networking (WiSPNET)*, 2019, pp. 140–145, doi: 10.1109/WiSPNET45539.2019.9032873.

[23] L. d. S. Costa and R. A. A. de Souza, "Performance of blind cooperative spectrum sensing under impulsive noise," in *2020 IEEE Latin-American Conference on Communications (LATINCOM)*, 2020, pp. 1–6, doi: 10.1109/LATINCOM50620.2020.9282340.

[24] A. Mehrabian, M. Sabbaghian, and H. Yanikomeroglu, "Spectrum sensing for symmetric α-stable noise model with convolutional neural networks," *IEEE Transactions on Communications*, vol. 69, no. 8, pp. 5121–5135, 2021, doi: 10.1109/TCOMM.2021.3070892.

[25] S. Lee, S. R. Park, Y. H. Kim, and I. Song, "Spectrum sensing for cognitive radio network with multiple receive antennas under impulsive noise environments," *Journal of Communications and Networks*, vol. 23, no. 3, pp. 171–179, 2021, doi: 10.23919/JCN.2021.000016.

[26] D. A. Guimarães, *Digital Transmission: A Simulation-Aided Introduction with VisSim/Comm*. Berlin Heidelberg, Germany: Springer Verlag, 2009, doi: 10.1007/978-3-642-01359-1.

[27] L. G. B. Guedes and D. A. Guimarães, "Sensoriamento espectral com receptor por conversão direta sob ruído impulsivo," in *XL Simpósio Brasileiro de Telecomunicações e Processamento de Sinais (SBrT 2022)*, Santa Rita do Sapucaí, MG, Brazil, Sep. 2022, doi: 10.14209/sbrt.2022.1570808562.

[28] D. A. Guimarães, R. A. A. De Souza, and A. N. Barreto, "Performance of cooperative eigenvalue spectrum sensing with a realistic receiver model under impulsive noise," *Journal of Sensor and Actuator Networks*, vol. 2, no. 1, pp. 46–69, 2013, doi: 10.3390/jsan2010046.

[29] Y. Luo, "Cooperative, cognitive and coordinated communications for underwater acoustic networks," 2015, Doctoral Thesis, University of Connecticut, USA. [Online]. Available: https://opencommons.uconn.edu/dissertations/983

[30] J. Xiaolin, T. Zhengyu, and W. Ronghui, "A novel cooperative spectrum signal detection algorithm for underwater communication system," *J Wireless Com Network*, Oct. 2019, doi: 10.1186/s13638-019-1550-x.

[31] C. Yun, "An underwater cooperative spectrum sharing protocol for a centralized underwater cognitive acoustic network," *Sensors*, vol. 22, no. 15, 2022, doi: 10.3390/s22155754.

[32] M. Shao and C. Nikias, "Signal processing with fractional lower order moments: stable processes and their applications," *Proceedings of the IEEE*, vol. 81, no. 7, pp. 986–1010, 1993, doi: 10.1109/5.231338.

[33] G. E. P. Box, G. M. Jenkins, G. C. Reinsel, and G. M. Ljung, *Time Series Analysis: Forecasting and Control*, 5th ed., ser. Forecasting and Control Series. Hoboken, New Jersey, USA: Prentice Hall, 2016, doi: 10.1111/jtsa.12194/978-1-118-67502-1.

[34] A. Mahmood, "The αSGNm toolbox for Matlab," July 2018. [Online]. Available: https://github.com/ahmd-mahm/alpha-SGNm\#the-\%CE\%B1sgnm-matlab-toolbox

[35] R. Wang and M. Tao, "Blind spectrum sensing by information theoretic criteria for cognitive radios," *IEEE Trans. Veh. Technol.*, vol. 59, no. 8, pp. 3806–3817, 2010, doi: 10.1109/TVT.2010.2065250.

[36] R. Gao, Z. Li, H. Li, and B. Ai, "Absolute value cumulating based spectrum sensing with Laplacian noise in cognitive radio networks," *Wireless Personal Communications*, vol. 83, July 2015, doi: 10.1007/s11277-015-2457-4.

[37] D. A. Guimarães, "Simple SNR wall calculation by equating the medians of the detector's test statistic," in *XL Simpósio Brasileiro de Telecomunicações e Processamento de Sinais (SBrT 2022)*, Santa Rita do Sapucaí, MG, Brazil, Sep. 2022, doi: 10.14209/sbrt.2022.1570808158.

[38] D. A. Guimarães, "Robust test statistic for cooperative spectrum sensing based on the Gerschgorin circle theorem," *IEEE Access*, vol. 6, pp. 2445–2456, 2018, doi: 10.1109/ACCESS.2017.2783443.

[39] ——, "Gini index inspired robust detector for spectrum sensing over ricean channels," *Electronics Letters*, Nov. 2018, doi: 10.1049/el.2018.7375.

[40] ——, "Pietra-Ricci index detector for centralized data fusion cooperative spectrum sensing," *IEEE Transactions on Vehicular Technology*, vol. 69, no. 10, pp. 12 354–12 358, 2020, doi: 10.1109/TVT.2020.3009440.

[41] D. Ramirez, J. Via, I. Santamaria, and L. L. Scharf, "Locally most powerful invariant tests for correlation and sphericity of gaussian vectors," *IEEE transactions on information theory*, vol. 59, no. 4, pp. 2128–2141, 2013, doi: 10.1109/TIT.2012.2232705.

[42] The Institute of Electrical and Electronic Engineers, IEEE, "IEEE 802 Part 22: Cognitive Wireless RAN Medium Access Control(MAC) and Physical Layer (PHY) Specifications: Policies and Procedures for Operation in the TV Bands," 2011. [Online]. Available: http://standards.ieee.org/getieee802/download/802.22-2011.pdf.

[43] R. G. Newcombe, "Two-sided confidence intervals for the single proportion: comparison of seven methods," *Statistics in Medicine*, vol. 17, no. 8, pp. 857–872, 1998, doi: 10.1002/(SICI)1097-0258(19980430)17:8<857::AID-SIM777>3.0.CO;2-E.

[44] D. A. Guimarães and E. J. T. Pereira, "Performance of detectors for spectrum sensing using a direct-conversion receiver model," May 2021. [Online]. Available: https://codeocean.com/capsule/1153872/tree/v1

[45] F. Ruiz-Vega, M. C. Clemente, P. Otero, and J. F. Paris, "Ricean shadowed statistical characterization of shallow water acoustic channels for wireless communications," 2011, doi: 10.48550/ARXIV.1112.4410.

Luiz Gustavo Barros Guedes received the BSc (2019) degree in Telecommunications Engineering from the National Institute of Telecommunications (Inatel), Brazil. He is working towards the MSc degree and works as a DWDM Networks Specialist at Inatel. His research interests are digital transmission, signal processing, mobile communications, dynamic spectrum access, probability and statistics.

Dayan Adionel Guimarães received the MSc (1998) and the PhD (2003) degrees in Electrical Engineering from the State University of Campinas (Unicamp), Brazil. He is a Researcher and Senior Lecturer with the National Institute of Telecommunications (Inatel), Brazil. His research interests are the general aspects of wireless communications, specifically radio propagation, digital transmission, dynamic spectrum access and signal processing applied to telecommunications.